Available online at www.sciencedirect.com
SCIENCE DIRECT
Journal of Power Sources 146 (2005) 464–468
JOURNAL OF POWER SOURCES
www.elsevier.com/locate/jpowsour

Silver alloying effect on the electrochemical behavior of Si–Zr thin film anodes

Kwan-Soo Lee, Young-Lae Kim, Sung-Man Lee *

Department of Advanced Materials Science and Engineering, Kangwon National University, Chunchon, Kangwon-Do 200-701, South Korea

Available online 1 June 2005

Abstract

To improve the electrochemical performance of Si–Zr thin films, we have investigated the effect of the replacement of Zr by Ag in the films. The Si–Zr–Ag thin films were prepared by co-sputtering from each pure target and then analyzed for structure, composition and electrochemical performance. The Ag-containing films show a plateau like region in the charge–discharge profiles, while the steep slopes are seen in the Si–Zr film. The Si–Zr–Ag films also show high capacity and good rate capability compared to the Si–Zr film, maintaining a comparable capacity retention with cycles. The improved electrochemical performance of Si–Zr–Ag films is attributed to the highly dispersed Si phase in the film, which was induced by formation of Zr–Ag bonds, and the lower impedance exerted by Ag alloying.

Keywords: Lithium ion battery; Thin film battery; Thin film anode; Si–Zr–Ag; Si–Zr

1. Introduction

In recent years, much research has been undertaken to search alternatives to metallic lithium anode in lithium rechargeable thin film batteries. Li–Sn and Li–Si systems have received great attention due to their large capacities ($Li_{4.4}Si$: 4200 mAh g^{-1}, $Li_{4.4}Sn$: 990 mAh g^{-1}). However, the main problem of these alloy systems is the large volume change occurring during Li insertion/extraction cycling, which leads to mechanical cracking and poor cycling stability of the electrodes [1–3]. It has been reported that the alloying of active and inactive elements could enhance the electrochemical performance of those alloy systems when the active alloying elements are finely dispersed with an inactive component in a matrix [4–7]. On the other hand, it is believed that a strong affinity between active and inactive components of alloys is required for the structural stability of the alloy electrodes.

Recently, the Si–Zr alloy system has been proposed as promising anode material for lithium rechargeable microbatteries because of its large negative heat of mixing of the constituent elements [8]. The electrochemical tests on Si–Zr thin film electrodes have revealed that the excellent cycling stability is achieved at the expense of a reversible capacity when the Zr content increases as reported in Ref. [8]. At this point, it should be noted that the $Si_{60}Zr_{40}$ electrode, showing excellent cycling performance, exhibited steeply sloping charge and discharge profiles without any potential plateaus. The steep slopes of the potential profiles indicate that the strong bonding of Zr atoms with Si atoms prevents Si from alloying large amount of Li, which results in the reduction of reversible capacity. Moreover, for an alternative to metallic lithium for the negative electrode in lithium ion cells, it is required to have small change in free energy for the insertion reaction, i.e., small potential changes relative to metallic lithium.

The purpose of this paper is to investigate the influence of the alloy composition changing on the electrochemical characteristics of Si–Zr thin film system. We decided first to replace partially Zr by Ag in $Si_{60}Zr_{40}$ and conduct a study on the $Si_{60}Zr_{40-x}Ag_x$ ternary system. Ag is thermodynamically immiscible with Si, but active towards Zr. Therefore, it is expected that the addition of Ag would affect the atomic distribution during thin film deposition, which induces a change in the reversible capacity and the shape of charge–discharge curves.

* Corresponding author. Tel.: +82 33 250 6266; fax: +82 33 242 6256.
E-mail address: smlee@kangwon.ac.kr (S.-M. Lee).

0378-7753/$ – see front matter © 2005 Elsevier B.V. All rights reserved.
doi:10.1016/j.jpowsour.2005.03.051

2. Experimental

Si–Zr–Ag thin films were deposited on Cu substrate with 12 mm diameter by simultaneous sputtering of separate targets, Si, Zr and Ag using dc magnetron sputtering method.

The power during deposition was varied for each target to produce the desired stoichiometries. The thickness of the films was about 150 nm. Chemical composition and stoichiometry of the films were examined using energy-dispersive spectroscopy (EDS) and X-ray photoelectron spectroscopy (XPS). X-ray diffraction (XRD) was used to examine the crystallinity of the films.

Electrochemical tests were performed in coin type half cells using metallic lithium as both reference and counter electrodes. The electrolyte was a 1 M $LiPF_6$ dissolved in a 50:50 (vol.%) mixture of ethylene carbonate (EC) and diethyl carbonate (DEC) (provided by Cheil Industries, Inc., South Korea). All cells were galvanostatically tested at 30 °C between 0 and 1.5 V versus Li/Li^+.

3. Results and discussion

The as-deposited Si–Zr–Ag thin films seem to have amorphous structure because no peak in the XRD patterns is observed (data not shown here).

Table 1 shows the relative atomic concentrations of Si–Zr–Ag films given by EDS and XPS. The results obtained from the XPS analysis reveal that there are high oxygen contents in the as-deposited Si–Zr–Ag thin films. It is suggested here that the majority of the oxygen is largely induced from oxygen resulting from the vacuum (base pressure: 2×10^{-6} torr) condition used in the deposition process. The elements with strong chemical affinity toward oxygen, especially Zirconium, can very easily adsorb a large amount of oxygen. It seems that the oxygen content in the film slightly decreases with replacing Zr by Ag.

XPS spectra of the Si2p, Zr3d, Ag3d regions obtained after sputter-etching from an as-deposited films are shown in Figs. 1–3. In each of those films, Si2p spectra show peaks at 99.35 and 102.8 eV (Fig. 1). The peak at 102.8 eV, 0.7 eV lower than for the stoichiometric SiO_2 is indicative of SiO_x [9], and the peak at 99.35 eV is resolved into two sub-peaks, one at 99.2 eV corresponding to pure silicon, and a higher

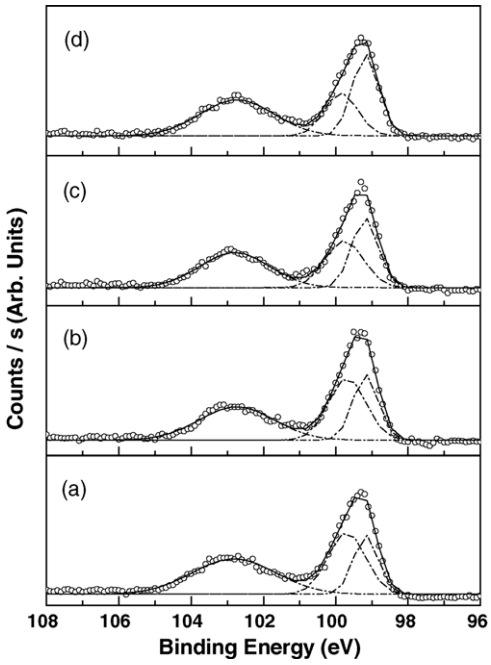

Fig. 1. XPS spectra of Si2p region in the Si–Zr–Ag and Si–Zr thin films: (a) Si–Zr thin film; (b) sample A; (c) sample B; (d) sample C.

binding energy peak around 99.7 eV resulting from probably silicide. It appears that the peak area at 99.2 eV corresponding to pure silicon increases with Ag content in the film. However, it is worthwhile to note that it is difficult to identify the binding state of Si, because the peak position of Si2p in silicide is similar that of pure Si [9].

Fig. 2 shows the Zr3d spectra. The peaks at 179.1 and 181.4 eV are expected to be the spectra of Zr in Zr–silicide and the peaks of binding energy, 183.4 and 185.8 eV, are ascribed to Zr oxide or Si–O–Zr bonds [9,10]. The peak intensities of those binding states decrease with the increase of Ag content to replace Zr in the films.

XPS spectra of Ag in the Si–Zr–Ag films are shown in Fig. 3, in which the spectra in Ag and ZrAg films, prepared to use as a reference, are compared. It can be seen that the Ag3d peak positions in Si–Zr–Ag films are consistent with Ag content in the films, which is similar to those in ZrAg film. In addition, compared with the peak positions of pure Ag, those in Si–Zr–Ag films are slightly shifted to a higher binding energy. Considering that Ag is thermodynamically

Table 1
Composition of the Si–Zr–Ag and Si–Zr thin films

Sample	Characterization method	Atomic concentration Si Zr Ag O	Si/(Zr–Ag) ratio
Si–Zr thin film	XPS	35.88 24.12–40.00	1.4875
A	XPS	36.44 20.87 04.26 38.43	1.4500
B	XPS	37.20 18.14 06.54 38.11	1.5072
C	XPS	37.14 14.71 10.70 37.45	1.4616
Si–Zr thin film	EDS	59.85 40.15	1.4906
A	EDS	59.92 33.05 07.03	1.4905
B	EDS	60.05 29.28 10.67	1.5018
C	EDS	60.21 23.85 15.94	1.5131

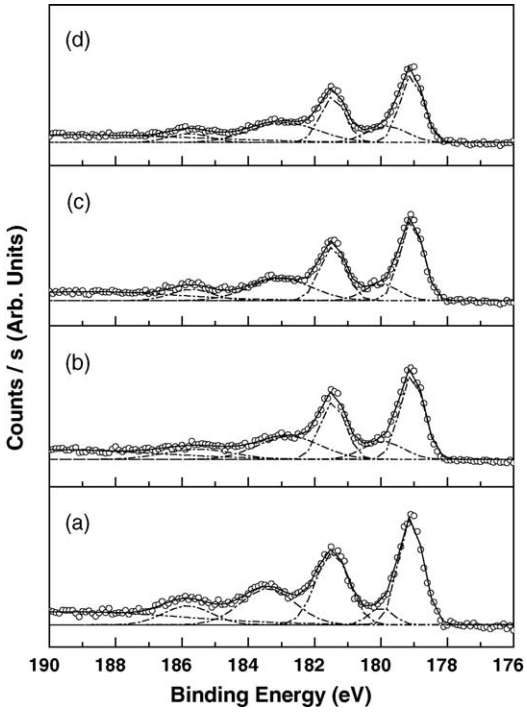

Fig. 2. XPS spectra of Zr3d region in the Si–Zr–Ag and Si–Zr thin films: (a) Si–Zr thin film; (b) sample A; (c) sample B; (d) sample C.

immiscible with Si, the result indicates the presence of Zr–Ag bonds in the Si–Zr–Ag films.

Fig. 4 shows the second charge–discharge curves for the Si–Zr–Ag thin film electrodes. For comparison, those of the Si–Zr thin film are also shown. When the Zr in the film is

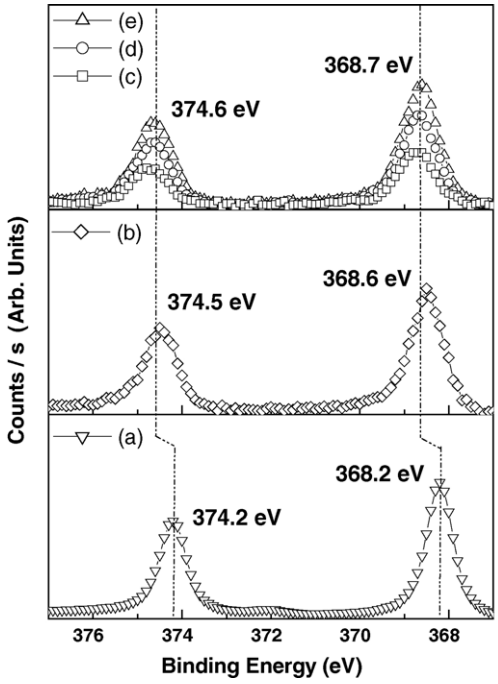

Fig. 3. XPS spectra of Ag3d region in the Si–Zr–Ag and Si–Zr thin films: (a) Ag thin film; (b) ZrAg thin film; (c) sample A; (d) sample B; (e) sample C.

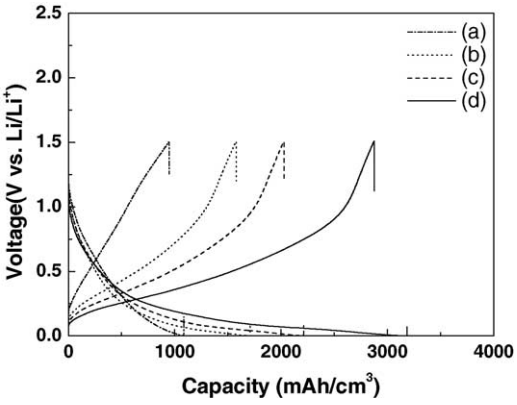

Fig. 4. The discharge/charge curves for the second cycle of the Si–Zr–Ag and Si–Zr thin film electrodes: (a) Si–Zr thin film; (b) sample A; (c) sample B; (d) sample C.

replaced by Ag, the charge plateau regions become visible, which leads to the capacity increase. In the case of Si–Zr film electrode, the voltage profiles have steep slopes. This behavior is apparent in the d*Q*/d*V* plots versus potential for the same cells as in Fig. 4. With increasing the Ag content in the Si–Zr–Ag films, the differntial capacity peaks become sharper and more well defined in both charge and discharge, while the Si–Zr film shows very smooth curves (Fig. 5). This indicates that the Li–Si alloying reaction in Si–Zr–Ag film electrodes is enhanced with the increase of the Ag content, resulting from the Si phase induced by the formation of Zr–Ag bonds as confirmed from the XPS data illustrated in Figs. 1–3. It is considered that the formed Si phase would be highly dispersed in the film.

The strong bonding of Ag atoms with Zr atoms may limit lithium alloying with Ag to form Li–Ag alloys.

Fig. 6 shows the discharge and charge capacities at the first cycle as a function of the thickness of the Si–Zr–Ag film (sample C). The first discharge capacity and the first charge capacity increase in proportion to the film thickness, but the irreversible capacity loss is not dependent on the film thickness. This means that the irreversible capacity observed in

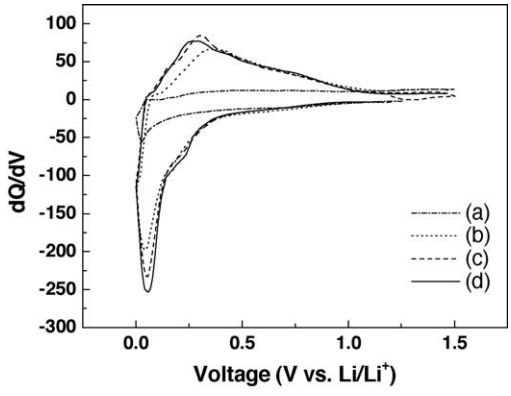

Fig. 5. The differential capacity vs. voltage for the second cycle of the Si–Zr–Ag and Si–Zr thin film electrodes: (a) Si–Zr thin film; (b) sample A; (c) sample B; (d) sample C.

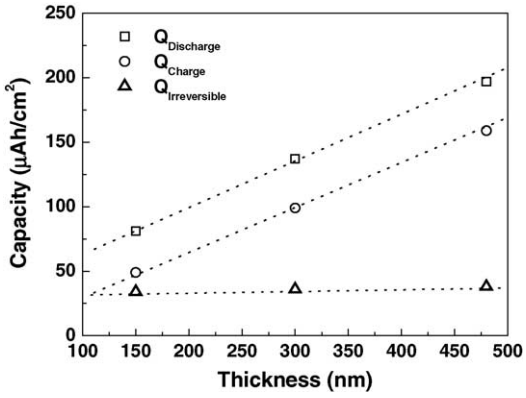

Fig. 6. Discharge/charge capacity and irreversible capacity for the first cycle of the Si–Zr–Ag thin film electrode (sample C) as a function of film thickness.

the Si–Zr–Ag film electrode is due to the interfacial reaction between the electrode surface and the liquid electrolyte rather than the intrinsic bulk characteristics.

Fig. 7 shows the normalized capacities of Si–Zr–Ag and Si–Zr thin films when cells were galvanostatically charged and discharged with different current densities. In the first five cycles, the current density was 30 $\mu A\,cm^{-2}$, then the current density increased to 50 $\mu A\,cm^{-2}$ in the second five cycles, and in the third and fourth five cycles to 100 $\mu A\,cm^{-2}$ and 250 $\mu A\,cm^{-2}$, respectively. When the current density increased, the Si–Zr–Ag samples with higher Ag content showed higher relative capacities. Presumably, the improved capacity retention at the higher rate could be associated with the lower impedance exerted by Si–Zr–Ag films.

Impedance spectra of Si–Zr–Ag and Si–Zr film electrodes after discharge to 0.0 V were measured and plotted as Nyquist plots in Fig. 8. The spectra shows a semicircle at high frequency and an inclining line at lower frequency. The semicircle at high frequency is associated with the impedance of Li ion migration through the surface film. Si–Zr–Ag film with higher Ag content shows a lower resistance for the Li ion transport through the surface film. This may be the result of higher promotion for the Li ion migration exhibited by the

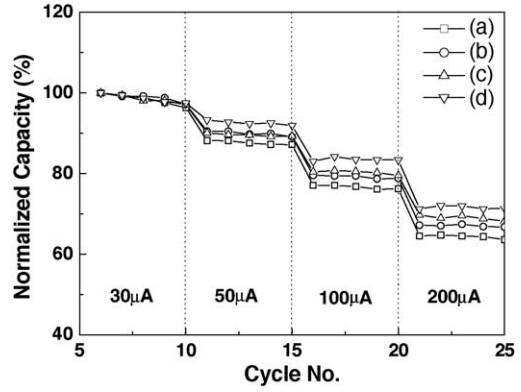

Fig. 7. The variation of normalized charge capacity as a function of current density for the Si–Zr–Ag and Si–Zr thin films: (a) Si–Zr thin film; (b) sample A; (c) sample B; (d) sample C.

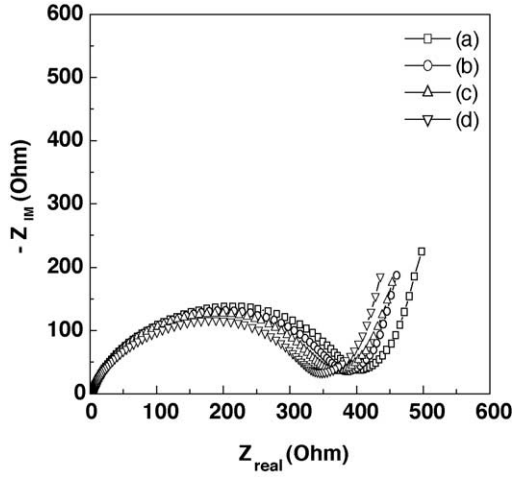

Fig. 8. Electrochemical impedance spectra of the Si–Zr–Ag and Si–Zr thin film electrodes: (a) Si–Zr thin film; (b) sample A; (c) sample B; (d) sample C before measurement, the electrodes were first discharged to 0.0 V, then allowed to relax at open-circuit for 0.5 h.

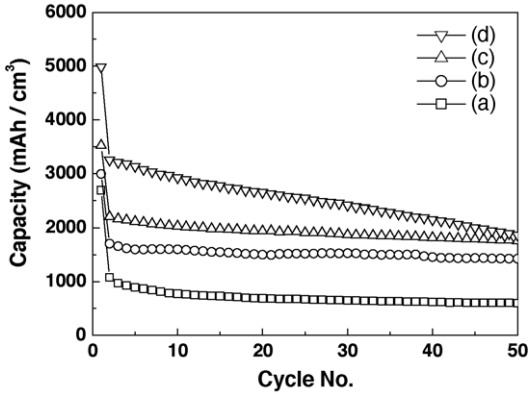

Fig. 9. Discharge capacity vs. cycle number of the Si–Zr–Ag and Si–Zr thin film: (a) Si–Zr thin film; (b) sample A; (c) sample B; (d) sample C.

alloying with Ag. However, the detailed mechanism is not clear at present.

Fig. 9 shows the capacity versus cycle number of the Si–Zr–Ag and Si–Zr thin film electrodes. The cycling performance of the Ag-containing films (samples A and B) is comparable to the Si–Zr film, and their capacities are higher than for Si–Zr electrode. In the case of sample C with highest Ag content, the cycling stability is worse than that of the Si–Zr sample, while is shows the largest capacity. The electrochemical properties would be further improved by a thorough optimization of the alloy composition.

4. Conclusions

In this paper, electrochemical results for Si–Zr–Ag films produced by co-sputtering from Si, Zr and Ag targets have been presented, and compared with those of Si–Zr film. As the result of the partial replacement of Zr by Ag in Si–Zr film, the charge–discharge potential profiles show a plateau like region instead of the steep slopes in Si–Zr film, which

leads to the reversible capacity increase. This is attributed to the Si phase induced by the formation of Zr–Ag bonds as confirmed from the XPS analysis. The Si–Zr–Ag films also showed good rate capability compared to the Si–Zr film, while the cycling stability is comparable.

Acknowledgement

This work was supported by the Korean Ministry of Science and Technology through the research program for "National Research Laboratory".

References

[1] J.O. Besenhard, P. Komenda, A. Paxinos, E. Wudy, M. Josowicz, Solid State Ionics 18–19 (1986) 823.
[2] J.O. Besenhard, M. Hess, P. Komenda, Solid State Ionics 40–44 (1990) 525.
[3] S.J. Lee, J.K. Lee, S.H. Chung, H.Y. Lee, S.M. Lee, H.K. Baik, J. Power Sources 97–98 (2001) 191.
[4] W.J. Weydanz, M. Wohlfahrt-Mehrens, R.A. Huggins, J. Power Sources 81–82 (1999) 237.
[5] G.X. Wang, L. Sun, D.H. Bradhurst, S. Zhong, S.X. Dou, H.K. Liu, J. Power Sources 88 (2000) 278.
[6] J. Yang, M. Winter, J.O. Besenhard, Solid State Ionics 90 (1996) 281.
[7] O. Mao, R.A. Dunlap, I.A. Courtney, J.R. Dahn, J. Electrochem. Soc. 145 (1998) 4195.
[8] S.J. Lee, H.Y. Lee, H.K. Baik, S.M. Lee, J. Power Sources 119–121 (2003) 113.
[9] J.F. Moulder, W.F. Sticklem, P.E. Sobol, K.D. Bomben (Eds.), Handbook of X-ray Photoelectron Spectroscopy, Perkin-Elmer Corporation, 1992.
[10] H. Ahn, H.W. Chen, D. Landheer, X. Wu, L.J. Chou, T.S. Chao, Thin Solid Films 455456 (2004) 318.